Applied Ocean Research 160 (2025) 104628

Contents lists available at ScienceDirect

Applied Ocean Research

journal homepage: www.elsevier.com/locate/apor

Power optimization modelling as a computational tool for power take off design in wave energy converters

Marcos Blanco [a,*], Isabel Villalba [b], Marcos Lafoz [a], Jorge Nájera [a], Gustavo Navarro [a], Miguel Santos-Herrán [c]

[a] CIEMAT (Centro de Investigaciones Energéticas, Medioambientales, y Tecnológicas), Avda. Complutense, no.40, Madrid CP28040, Spain
[b] ULPGC (Universidad de Las Palmas de Gran Canaria), Calle Juan de Quesada, 30, Las Palmas de Gran Canaria CP35001, Spain
[c] Carnegie Technologies Spain S.L., Calle Claudio Coello, 24 – 4A2, Madrid CP28001, Spain

ARTICLE INFO

Keywords:
Wave to wire
Power take-off
Optimisation
Losses model
Modular generator

ABSTRACT

This study presents a computational tool called Power Take-Off Optimisation Modelling (POM), a methodology for optimizing the design parameters of the Power Take-Off (PTO) in wave energy converters (WECs). POM uses a control optimization algorithm based on a differential evolution multi-objective approach to maximize the electrical power extracted by WECs while minimizing design costs.

The methodology integrates a wave-to-wire (W2W) model in the time domain, including a PTO loss model. It also considers the sea states where WECs operate, and constraints related to the PTO rated force. These features allow a comprehensive evaluation of the electrical energy generated and the optimization of PTO design parameters.

POM has been applied to a real case study involving a linear generator-based PTO operating under different sea states. The analysis includes four WEC technologies and two sea states to assess the tool's effectiveness.

Results show that PTO length influences not only CAPEX minimization but also optimal modular system design. Additionally, a sensitivity analysis indicates that the number of modules required to meet force requirements is not significantly affected by PTO efficiency.

In conclusion, POM is a versatile support tool for technology developers and researchers, helping optimize PTO design to balance WEC manufacturing costs and generated power.

1. Introduction

In the search for solutions tomitigate climate change, marine renewable energies have emerged as a key element in the transition to a new energy model. Among marine renewable energies, wave energy is one of the most promising options. The vast global resource (Mørk et al., 2010; Gunn and Stock-Williams, 2012), the technological advances in wave energy converters (WECs) over the last decade (de and Falcão, 2010; Pecher and Kofoed, 2017),and the successful implementation of numerous research and development (R&D) projects (Conill, 2022) have positioned wave energy as a viable future option. However, WECs still face some challenges in achieving economic viability. Reports (Cagney, 2022; Europe 2023) outline objectives for wave energy in Europe by 2030, proposing an installed and grid connected capacity of 496MW. The reports (Cagney, 2022; Europe 2023; Tan et al., 2021) also suggest that optimized WEC solutions can reduce the Levelized Cost Energy (LCOE) to approximately 110 €/MWh without compromising efficiency.

Among the costs contributing to the LCOE, the manufacturing cost (CAPEX) plays a significant role. A key component of CAPEX is the manufacture of the energy extraction system or power take-off (PTO). Economic studies on WECs (Guo et al., 2023; Chang et al., 2018; Tan et al., 2021) identify CAPEX as a critical factor, emphasizing the optimization of WEC rated design characteristics as essential for reducing total costs.

Several previous studies have focused on methodologies to optimize PTO designs for WECs (Balaji et al., 2020; Saveca et al., 2022; Amini et al., 2022). These optimization studies have primarily aimed to maximize WECs generated power by tuning the design parameters of

During the preparation of this work the author(s) used ChatGPT in order to help to improve the language and readability. After using this tool/service, the author(s) reviewed and edited the content as needed and take(s) full responsibility for the content of the publication.

* Corresponding author.
E-mail address: marcos.blanco@ciemat.es (M. Blanco).

https://doi.org/10.1016/j.apor.2025.104628
Received 20 January 2025; Received in revised form 13 May 2025; Accepted 20 May 2025
Available online 2 June 2025

PTOs. Other studies explore multi-objective optimization, balancing maximum power generation and cost reduction of the complete WEC (He et al., 2022; He et al., 2022; Sirigu et al., 2020; Blanco et al., 2019; 2021; 2015).

The optimization method proposed in the Power Take-Off Optimization Modelling (POM) is based on a time domain Wave-to-Wire (W2W) model (Alves, 2012), providing a versatile numerical tool applicable to different WECs. Time domain hydrodynamic models have been studied for decades in works such as (Cummins, 1962; Wehausen, Jan. 1967), which analyse oscillating movements, accompanied with other foundational modelling studies (Yu and Maceda, 1991; Yu and Falnes, 1995). The POM presented in this paper expands and adapts the model to include the Power take-off (PTO) characteristics, as described in (Faiz and Nematsaberi, 2017), including rated parameters, efficiency using a loss model, and operation constraints. In addition, the optimization algorithm considers these efficiency factors and constraints to maximize electric power rather than mechanical power (Blanco et al., 2019).

Various types of Power Take-Off (PTO) systems have been developed for wave energy conversion, including hydraulic, pneumatic, and mechanical systems—which typically involve intermediate energy conversion stages—as well as direct-drive technologies based on linear electric generators. Wave energy projects at the prototype and pilot stages commonly employ these different PTO configurations (Tan et al., 2022; Ahamed et al., 2020), reflecting both the varying levels of technological maturity and the distinct advantages and limitations associated with each approach. For instance, mechanical PTO systems, such as those based on rack-and-pinion mechanisms, can offer high efficiency and high motor-constant values (force-current ratios) (Yang et al., 2024; Markel Penalba and Ringwood, 2016) and allow for the integration of intermediate energy storage solutions like flywheels. However, they often suffer from relatively short lifetime and high gear-ratio values (conversion low linear velocities in high rotational speeds) (Ahamed et al., 2020).

The present work focuses on direct-drive PTO systems, as linear electric generator technologies (Ahamed et al., 2022; Zhang et al., 2023) offer interesting advantages. These include the elimination of intermediate mechanical interfaces, resulting in lower maintenance costs and comparatively high efficiency. Nevertheless, such systems also present challenges, notably the low translator speed compared to the rotational speed of conventional generators, which results in a lower power-to-weight ratio and lower motor-constant. Additionally, robust structural components are required to withstand magnetic attraction forces (Ahamed et al., 2022; Zhang et al., 2023; Maria-Arenas et al., 2019). Despite these challenges, This PTO topology minimizes potential system failures across conversion stages and improves control of the PTO extraction force (Davidson et al., 2018; El Montoya Andrade et al., 2014), enhancing overall system efficiency.

POM also considers the sea states at the WECs installation sites, as the wave climate is a key design parameter to align PTO characteristics with the design problem based on the specific location (Blanco et al., 2015). In addition to maximize the electric power extraction, the POM introduces a new objective function: minimizing PTO manufacturing costs. This multi-objective algorithm enables POM to advance the state of the art in the optimization tools for the PTO design in WECs.

It is also important to point out that PTO efficiency should be integrated into control algorithms to maximize electrical power generation, rather than mechanical power (Blanco et al., 2019; 2021; 2015). Optimizing mechanical energy leads the system to operate away from optimal electrical performance. The W2W model proposed in POM incorporates PTO system constraints, such as the force exertion limits (Blanco et al., 2011; Tedeschi and Molinas, 2012), which affect both the power generated and equipment cost. Consequently, the model can define the main the linear generator characteristics for a specific WEC (Blanco et al., 2011).

As an example, this paper applies POM to eight case studies -combination of four WEC technologies and two sea locations. This work is based on the SEATITAN project (Surging Energy Absorption Through Increasing Thrust And efficientNcy) (Europe 2025) funded by the European H2020 Programme, GA No.764014. One of SEATITAN's objectives was the design of a versatile, modular and scalable PTO that could be integrated into four WECs technologies, as SEATITAN consortium included four WEC technology developers (CORPOWER Homepage 2025; HYDROCAP ENERGY homepage 2025; CENTIPOD homepage 2025; WEDGE Global S.L. Homepage 2025). The project also involved the design of a novel azimuthal linear switched reluctance generator (AMSRM) (Blanco et al., 2021), developed in a multi-translator configuration, adaptable to varying stroke and force requirements.

Once the PTO design objective was achieved, the focus shifted to identify solutions to maximize WEC electrical power output while minimizing manufacturing costs. To achieve this, POM obtains the optimal AMSRM force and stroke values for the eight defined case studies while selecting the appropriate number of AMSRM modules for each case.

The paper is organized as follows: Section 2 provides an overview of the POM methodology, addressing its key parts: the time domain hydrodynamic model (W2W) (Section 2.1), the mathematical PTO loss model (Section 2.2) and the multi-objective optimization algorithm (Section 2.3). Sections 2.1 and 2.2 are described using a particular WEC case study - Wedge Global (WGwec) (WEDGE Global S.L. Homepage 2025) - selected from the SEATITAN project. This WEC technology has been simplified for better understanding of the POM methodology. Section 3 describes the analysis and results of applying POM to four WEC technologies and two different locations, demonstrating the adaptability to various PTO configurations. Section 4 discusses the results obtained from POM evaluation as PTO design tool. Finally, Section 5 presents the main conclusions of the study.

2. Power take-off optimisation model (POM)

The main POM phases are summarized in Fig. 1, Fig. 2. POM includes a W2W model in the time domain, which, besides the prime mover dynamic model, integrates a control strategy and a PTO loss model. The W2W model takes as input supra-parameters: the WEC and its location (sea states), meaning parameters that cannot change during

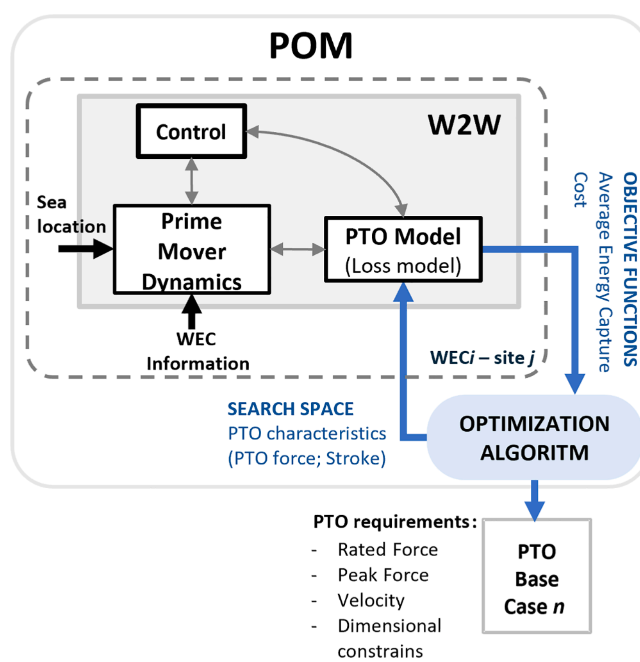

Fig. 1. Diagram and scheme of the problem optimization modelling (POM).

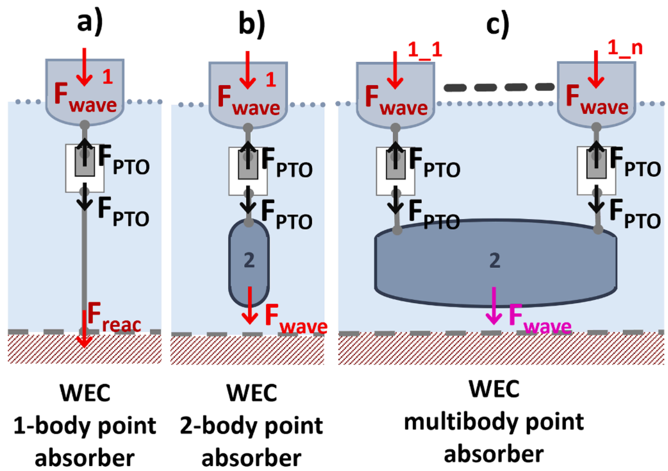

Fig. 2. Topology type WEC. (a) one-body point absorber. (b) two-body point absorber. (c) Multibody point absorber.

optimization. A nominal 85 % efficiency (electrical losses) is assumed, based on simulations and lab tests of the considered linear electrical generator (AMSRM) (Blanco et al., 2021).

POM also includes a multi-objective optimization algorithm based on a differential evolutionary algorithm (DE) (Price and Storn, 2025) adapted to solve multi-objective problems (MODE) (Mørk et al., 2010). The search space has two variables: PTO rated force and rated stroke, representing PTO topology characteristics. The optimization considers two objectives: maximizing PTO electrical power output and minimizing PTO fabrication costs (CAPEX).

Both the PTO loss model and W2W were developed in MATLAB©, widely used in industry for simulations. Since only basic libraries were used, migration to open-access platforms like OCTAVE or generating an open-access executable version is possible.

Sections 2.1–2.3 will explain in detail the POM subsystems and their main characteristics.

2.1. Description of the wave to wire time domain model of the prime mover

2.1.1. Time domain model

The W2W model represents the entire energy conversion chain, from wave device interaction to the resulting electrical energy, including models such as WEC model and PTO model. As a first step, the WEC model is based on linear wave theory and potential flow, and it is adapted from (Alves, 2012; Penalba and Ringwood, 2016). In essence, it is the application of Newton's second law, considering hydrodynamic and external forces.

This study considers the two-body point absorber as the selected WEC topology. It consists of: the top floater and the spar-plate (see Fig. 2b). Its dynamic performance is based on the relative movement between these two bodies, with the study focusing on movement restriction to the z-axis (heave movement). The prime mover's heave movement is used by the PTO to extract energy from ocean waves.

The W2W model in the time domain for a two-body point absorber is defined in Eqs. (1) and (2), where (1) corresponds to the floating body and (2) to the submerged body.

$$m_1 \cdot \frac{\delta^2 z_1}{\delta t^2} = \sum F = F_{mec_1} + F_{s1} + F_{r11} + F_{r12} + F_{mec_{12}} + F_{e,1} - F_{PTO}$$
$$= -R_{mec_1} \cdot \frac{\delta z_1}{\delta t} - S_1 \cdot z_1 - R_{r11} * \frac{\delta z_1}{\delta t} - R_{12} * \frac{\delta Z_2}{\delta t} - m_{ad11} \frac{\delta^2 z_1}{\delta t^2}$$
$$- m_{ad12} \cdot \frac{\delta^2 Z_1}{\delta t^2} - R_{mec_{12}} \cdot \left(\frac{\delta z_1}{\delta t} - \frac{\delta z_2}{\delta t}\right) + \left(F_{e,1} - F_{PTO}\right) \quad (1)$$

$$m_2 \cdot \frac{\delta^2 z_2}{\delta t^2} = \sum F = F_{mec_2} + F_{s2} + F_{r22} + F_{r12} + F_{mec_{12}} + F_{e,2} + F_{PTO}$$
$$= -R_{mec_2} \cdot \frac{\delta z_2}{\delta t} - S_2 \cdot z_2 - R_{r22} * \frac{\delta z_2}{\delta t} - R_{r12} * \frac{\delta z_1}{\delta t} - m_{ad22} \cdot \frac{\delta^2 z_2}{\delta t^2}$$
$$- m_{ad12} \cdot \frac{\delta^2 z_1}{\delta t^2} - R_{mec_{12}} \cdot \left(\frac{\delta z_1}{\delta t} - \frac{\delta z_2}{\delta t}\right) + \left(F_{e,2} + F_{PTO}\right) \quad (2)$$

Here, sub-index 1 corresponds to the floating body and sub-index 2 to the submerged body. The symbol * represents the convolution product and j represents the imaginary variable $\sqrt{-1}$. The forces and impedance represented are:

F_{ei} the excitation force to the "i" body,
R_{ri} the radiation resistance of the body due to body motion,
M_{adi} the added mass of the body i by the motion of the body,
R_{rij} , M_{asij} the mutual mechanical impedances,
R_{meci} the mechanical resistance,
M_i the total body mass,
S_i the coefficient of restoration or Archimedean force,
F_{PTO} the mechanical force developed by the electric generator.

This model accounts for the hydrodynamic terms of the fluid-body interactions, including the excitation force F_{ei} (which depends solely on the incident wave and not on the body's motion, and includes the force caused by both the incident and diffracted waves), and the radiation force F_{rij} (which depends on the motion or oscillation of the body in the fluid and represents the fluid's resistance to this motion, generating a radiated wave that dissipates energy).

The non-frequency dependent terms (M_i, S_i, R_{meci} y F_{PTO}) are directly determined from the device dimensions. On the other hand, the frequency-dependent terms (F_{ei}, $M_{adi,}M_{adij}$, R_{ri}, R_{rij}) are hydrodynamic coefficients of the floating bodies and depend only on the geometry of the WEC. In this study, the hydrodynamic coefficients were obtained by using the WAMIT BEM (boundary integral equation method) computational tool (Lee, 1995).

The excitation force (F_{ei}) is evaluated in time domain from the frequency-dependent coefficients and particularized to each profile of the free surface elevation (i.e. a free surface profile defined as a summation of a large number of sinusoidal waves, each with a specific frequency, a random phase, and amplitudes determined by a predefined spectral model a sea state). The radiation force (F_{rij}) is expressed commonly as a convolutional integral (Cummins, 1962) which use the values of the frequency-dependent coefficients (M_{adij}, R_{ri}, R_{rij}), and it is approximated by a state-space representation (Yu and Falnes, 1995) where its coefficients are obtained using Prony's method (Alves, 2012; Cummins, 1962; Wehausen, Jan. 1967; Yu and Maceda, 1991; Yu and Falnes, 1995; Faiz and Nematsaberi, 2017; Blanco et al., 2019).

The POM uses this time domain W2W model to evaluate the different solutions. Time domain models provide higher accuracy (compared to frequency domain models) when evaluating the energy extracted by the complete WEC (prime mover + PTO) (Alves, 2012; Hals et al., 2011; de Andrés et al., 2013), whose maximization is one of the objectives of the POM (see Section 2.4.2). In addition, it allows the consideration of non-linearities, such as the implementation of controls including PTO force limiting (see Section 2.3) (Blanco et al., 2019; Bechlenberg et al., 2023).

2.1.2. Frequency domain model

From the time domain model, a frequency domain model based on an electrical analogy is proposed in this subsection (Falnes, 2002). The approach of an electrical circuit will allow to express the magnitudes in phasors, and to apply the theorems and analysis of electrical engineering.

Eqs. (1) and (2) can also be represented using their analogue electrical circuit (see Eqs. (3) and (4)) in frequency domain. In this analogue circuit, each mechanical variable has an equivalent electrical variable.

forces are represented as voltages and velocities are equivalent to currents. Regarding impedances, mass corresponds to inductance, spring constants to the inverse of the capacitance and damping coefficients or mechanical resistances to electrical resistances (see Fig. 3). Eqs. (3) and (4) has been reformulated in frequency domain according to (Falnes, 2002) transforming variables in phasor form.

$$[R_{mec\_1}+R_{r11}]\cdot I_1+[j\cdot(-1/(\omega\cdot C_1)+\omega\cdot(L_1+L_{ad11}))]\cdot I_1+(R_{r12}+j\cdot\omega\cdot L_{\infty 12})\cdot I_2=Z_{11}\cdot I_1+Z_{12}\cdot I_2=\left(U_{e,1}-U_{PTO}\right) \tag{3}$$

$$[R_{mec_2}+R_{r22}]\cdot I_2+[j\cdot(-1/(\omega\cdot C_2)+\omega\cdot(L_2+L_{ad22}))]\cdot I_2+(R_{r12}+j\cdot\omega\cdot L_{\infty 12})\cdot I_1=Z_{12}\cdot I_1+Z_{22}\cdot I_2=\left(U_{e,2}+U_{PTO}\right) \tag{4}$$

R_{mec_i} is the mechanical equivalent resistance of the body i (the subindex "i" takes the value 1 for the floating body and 2 for the semi-submerged body),

R_{rij} is the radiation hydrodynamic resistance of the body i produced by the movement of the body j,

C_i is the capacity associated with the stiffness coefficient of the body i; L_i is the inductance associated with the mass of the body I,

L_{adij} is the added mass inductance of the body i produced by the movement of the body j,

U_{ei} is the excitation voltage of the body i; U_{PTO} is the voltage that represents the PTO force,

I_i is the current that represents the velocity of the body i; Z_{11} is the body 1 total impedance,

Z_{22} is the body 2 total impedance; and Z_{12} and Z_{21} the mutual impedances (Blanco et al., 2015)

Eqs. (3) and (4) can be expressed in matrix form (see (5)):

$$\begin{bmatrix} Z_{11} & Z_{12} \\ Z_{12} & Z_{22} \end{bmatrix}\cdot\begin{bmatrix} I_1 \\ I_2 \end{bmatrix}=\begin{bmatrix} U_{e,1}-U_{PTO} \\ U_{e,2}+U_{PTO} \end{bmatrix} \tag{5}$$

The analogue electric circuit of a two-body point absorber (Fig. 3b) can be simplified according to the Thevenin theorem (Grainger and Stevenson, 1994) (see (6) and (8)). This theorem allows to replace the WEC analogue electric circuit (see Fig. 3) of a 2-body WEC – composed by voltage sources and impedances - by an equivalent combination of a single voltage source (U_{TH}) in a series connection with a single impedance (Z_{TH}). The resultant circuit it is the analogue circuit of a one-body WEC (Blanco et al., 2019). From the PTO point of view, this simplified circuit is equivalent to the circuit diagram of a one-body point absorber from (Fig. 3a) (Blanco et al., 2015), where: U_{TH} is the Thevenin equivalent voltage – the open-circuit voltage - (6), I_{PTO} is the short circuit current (7), and Z_{TH} is the Thevenin equivalent impedance (8). These equations represent the simplified circuit.

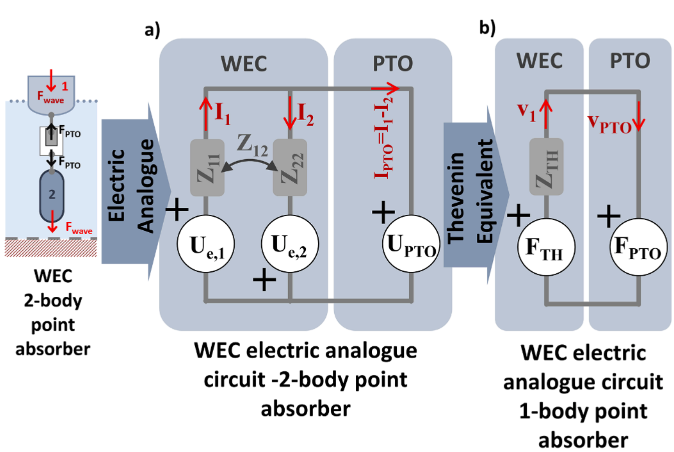

Fig. 3. Electric analogue Circuits (a) 2-Body WEC; (b) 1-Body WEC (Gunn and Stock-Williams, 2012) (applying Thevenin theorem).

$$U_{TH}=\left((Z_{11}+Z_{12})\cdot U_{e,1}-(Z_{22}+Z_{12})\cdot U_{e,2}\right)/(Z_{11}+Z_{22}+2\cdot Z_{12}) \tag{6}$$

$$I_{PTO}=\frac{(Z_{11}+Z_{12})}{\left(Z_{11}\cdot Z_{22}-Z_{12}^2\right)}U_{e,1}-\frac{(Z_{22}+Z_{12})}{\left(Z_{11}\cdot Z_{22}-Z_{12}^2\right)}U_{e,2} \tag{7}$$

$$Z_{TH}=\frac{U_{TH}}{I_{PTO}}=\frac{\left(Z_{11}\cdot Z_{22}-Z_{12}^2\right)}{(Z_{11}+Z_{22}+2\cdot Z_{12})}=\left(Z_{11}\cdot Z_{22}-Z_{12}^2\right)\cdot\left(Z_{11}^*+Z_{22}^*+2\cdot Z_{12}^*\right)\Big/|(Z_{11}+Z_{22}+2\cdot Z_{12})|^2 \tag{8}$$

This frequency domain approximation will be used in Section 2.3 to propose PTO energy extraction strategy.

2.2. Mathematical model of PTO losses

This section describes the PTO loss model and the energy extraction control subsystem. The PTO consists of an electrical linear generator and its power electronic converter, ideal for heaving point absorber WECs, as it converts linear motion into electricity without intermediaries (de and Falcão, 2010). The PTO loss model calculates the WEC electrical output and helps define its control strategy. Both are integrated into the W2W model (see Section 2.1).

In a mechanical W2W model, a detailed electric PTO model is often unnecessary due to faster electrical dynamics. Power electronic semiconductors switch in the kHz range, much higher than mechanical frequencies (Blanco et al.). A power loss model is used instead. For example, the PTO reaches rated current at rated velocity in 10–20 ms, while ocean wave periods last tens of seconds.

The PTO loss model is parametrized for the azimuthal linear switched reluctance generator (AMSRM) (Blanco et al., 2021), developed in the SEATITAN Project (Europe 2025). However, it can also apply to other linear generator types, like induction or permanent magnet synchronous generators.

The PTO loss model considers key technological factors (Carstensen, 2008).

- Magnetic losses: Foucault and hysteresis losses (Sadiku and Alexander, 2007)- depend on current oscillation frequency and stator-translator velocity (Torres et al., 2018). Negligible due to low displacement velocities.

- Electric losses: Joule losses (Sadiku and Alexander, 2007) in cables and generator coils, dependant on current. They account for ~95 % of total losses particularly relevant in linear generators, where high forces and low velocities lower efficiency compared to rotating generators.
- Power Electronic losses: Switching and conduction losses, dependent on current amplitude and frequency. Neglected due to high system efficiency.
- Mechanical losses: Friction losses (~1–2 %) based on tests with linear generators (Carstensen, 2008; Sadiku and Alexander, 2007; Torres et al., 2018; García et al., 2011). Negligible due to low velocity. .

The mechanical power output - P_{mech} (9) – and the WEC electrical power output - P_{elec} (10) - can be evaluated from previous Eqs. (1), (2). In addition, based on previous considerations, the conclusion is that the equation referring the total PTO power losses (11) can be simplified and only the term of electrical losses is considered (12).

$$P_{mech}(t) = F_{PTO}(t) \cdot \upsilon_{rel}(t) \tag{9}$$

$$P_{elec}(t) = P_{mech}(t) - P_{loss_{elec}}(t) \tag{10}$$

$$P_{loss}(t) = P_{loss_{mag}}(t) + P_{loss_{elec}}(t) + P_{loss_{electronic}}(t) + P_{loss_{mech}}(t) \tag{11}$$

$$P_{loss}(t) = P_{loss_{elec}}(t) = P_{Cu}(t) \tag{12}$$

Here, υ_{rel} is the WEC relative velocity and P_{loss} is power losses output, R'_{PTO} represents the losses in the PTO.

By incorporating Eqs. (9) and (12) into the development of (10), Eq. (13) summarizes the expression for the $P_{elec}(t)$ in the PTO loss model. This Eq. (13) will be used in the next Section (2.3) to set up a WEC control strategy that maximized P_{elec} instead of P_{mech}.

$$\begin{aligned} P_{elec}(t) &= P_{mech}(t) - P_{loss}(t) = F_{PTO}(t) \cdot \upsilon_{PTO}(t) - P_{Cu}(t) \\ &= F_{PTO}(t) \cdot \upsilon_{PTO}(t) - R_{Cu} \cdot I^2_{PTO}(t) \\ &= F_{PTO}(t) \cdot \upsilon_{PTO}(t) - R_{Cu} \cdot \left(\frac{F_{PTO_{rated}}}{I_{PTO_{rated}}} \right)^2 \cdot F^2_{PTO}(t) \\ &= F_{PTO}(t) \cdot \left(\upsilon_{PTO}(t) - R'_{Cu} \cdot F_{PTO}(t) \right) \end{aligned} \tag{13}$$

Here: P_{elec} is the PTO generated electric power,
P_{loss} is the total PTO power losses,
P_{cu} is the Joule effect losses (winding losses),
F_{PTO} is the PTO force,
υ_{PTO} is the relative velocity between the two parts of the linear generator PTO,
R_{cu} is the electric resistance of one phase of the PTO,
I_{PTO} is the electric current of one phase of the PTO. This term is developed in (Pecher and Kofoed, 2017), where $F_{PTO_{rated}}$ is the PTO nominal force
$I_{PTO_{rated}}$ is the PTO current nominal value,
R'_{cu} is the coefficient to calculate the winding losses of PTO.

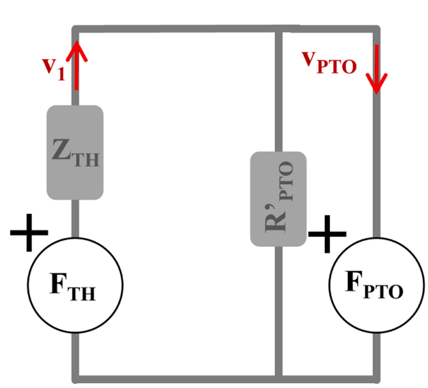

Fig. 4. Electrical circuit of a WEC including a PTO losses model.

2.3. Mathematical expressions of PTO energy extraction control

The complete PTO model could be formulated as an analogue electrical circuit (Conill, 2022; Cagney, 2022), also representing the power losses. The analogue circuit of the PTO can be integrated into the complete analogue circuit of the WEC (Fig. 4).

The electrical circuit represents a one-body WEC, however it is always possible to apply Thevenin's Theorem to formulate the dynamic behaviour for a two-body point absorber WEC (or even multi-body) as an analogue electrical dipole (Blanco et al., 2019; Sadiku and Alexander, 2007; Falnes, 1999), viewed from the WEC's perspective. The analogue electrical circuit of one-body WEC is depicted in Fig. 4, where the wave excitation force is represented by a voltage source, the mechanical hydrodynamic analogue impedance by an electric impedance in series and the PTO force by another voltage source. Finally, the PTO losses are modelled as a resistance in parallel with the PTO voltage source (14).

$$R'_{PTO} = \frac{1}{R'_{cu}} = \left(\frac{F_{PTO_{rated}}}{I_{PTO_{rated}}} \right)^2 \tag{14}$$

Once the WEC dynamic performance has been represented by an analogue electrical circuit, circuit analysis theory can be applied, using maximum electric power transfer theorem, to determine the value of the force (F_{PTO}) leading to the maximum power extracted from the waves, taking PTO losses into account. These equations are used by the energy extraction control subsystem.

$$Z_{PTO_{OPT}} = \left(\frac{R'_{PTO} \cdot Z_{WEC}}{R'_{PTO} + Z_{WEC}} \right)^* \tag{15}$$

$$F_{PTO_{OPT}} = \frac{F_{TH}}{2} \cdot \frac{R'_{PTO} \cdot Z^*_{TH}}{R'_{PTO} \cdot R_{WEC} + |Z_{TH}|^2} \tag{16}$$

$$\upsilon_{PTO_{OPT}} = F_{TH} \cdot \frac{1 + 2 \cdot Z^*_{TH}}{2 \cdot R'_{PTO} \cdot R_{TH} + 2 \cdot |Z_{TH}|^2} \tag{17}$$

Here the symbol ■* stands for complex conjugate, and "|■|" stands for absolute value.

In the case of a two-body WEC, F_{TH} is the equivalent force resultant from the application of the Thevenin's Theorem simplification. Z_{TH} is the total mechanical impedance, and $Z_{PTO_{OPT}}$ (15), $F_{PTO_{OPT}}$ (16) and $\upsilon_{PTO_{OPT}}$ (17) the optimal values obtained under optimally controlled conditions.

The above expressions can be formulated as a function of the PTO efficiency term -η- (18) and (19).

$$\eta = \frac{P_{elec}}{P_{mech}} = 1 - \frac{P_{loss}}{P_{mech}} = 1 - \frac{R'_{cu} \cdot F^2_{PTO}}{\upsilon_{PTO} \cdot F_{PTO}} = 1 - \frac{F_{PTO}}{R'_{PTO} \cdot \upsilon_{PTO}} \tag{18}$$

$$R'_{PTO}(\eta_{rated}) = \frac{1}{1 - \eta_{rated}} \cdot \frac{F_{PTO_{rated}}}{\upsilon_{PTO_{rated}}} \tag{19}$$

Here, η is the efficiency of the PTO in generator mode (18) and η_{rated} is the efficiency at rated force and velocity.

It is important to note that if R'_{PTO} (19) tends to an infinite value, the PTO has no losses, and the expressions coincide with those already developed in the Energy Maximizing Control (EMCs) theory, based on linear models (Davidson et al., 2018). Consequently, Eqs. (15), (16) and (17) can be translated into the following optimal control expressions in (20).

$$Z_{PTO_{OPT}} = Z^{*}_{TH};\ F_{PTO_{OPT}} = F_{TH} \cdot \frac{Z^{*}_{TH}}{R_{TH}};\ v_{PTO_{OPT}} = \frac{F_{TH}}{2 \cdot R_{TH}} \tag{20}$$

In addition, the $F_{PTO_{OPT}}$ should be limited to its rated value, due to its high impact in the energy extraction results (Tedeschi and Molinas, 2012; Genest et al., 2014; Blanco et al., 2019). The values obtained in (20) are used in time domain simulations of POM implementing a gain scheduling control strategy according to the WEC control methods described in (Hals et al., 2011), including a saturation in the force exerted by the PTO up to its rated value.

2.4. Description muti-objective optimisation algorithm

This section describes the multi-objective optimisation algorithm. A differential evolutionary algorithm (DE) (Price and Storn, 2025) has been modified and adapted to multi-objective problems (MODE) (Mørk et al., 2010).

The PTO main characteristics selection is posed as an optimization mathematical problem, and in this context, the objective functions and the variables of the search space has to be defined.

2.4.1. Search space variables

Due to the fact that the POM is used to determine the most appropriate PTO, the variables to be selected are the basic characteristics of this PTO topology: (1) the rated force -$F_{PTO_{rated}}$- and (2) the rated stroke -$S_{PTO_{rated}}$ -, constituting the search space of the optimization algorithm.

PTO force represents the force capacity of the real design of the PTO. The limitations of the PTO force are related to the mechanical limitations of the linear generator considered, as well as to the electric current limitations at the electric generator coils and the power electronic converter used to drive it.

2.4.2. Objective functions

The goal is to optimise (to maximise, in this case) the average electrical power generated and to optimise (to minimise, in this case) the generator cost. In this context, the two objective functions considered in the optimization problem are:

- The maximization of the generated power by the complete system.
- The minimization of the cost of the PTO.

The selection of optimization metrics for each specific problem is never trivial. In this case, one of the variables considered is the cost of the device to be sized (PTO). Given that this cost model can be challenging to capture, future work may analyse different metrics, such as more general metrics such as the capacity factor.

The average electrical power is evaluated using a W2W model (Sections 2.1 and 2.2), by simulating every relevant sea state in each scenario, determined by the WEC type and location. The generator cost is assessed as a function as shown in (21) and according to Blanco et al. (2019).

$$cost = C_0 + C_1 \cdot S_{PTO_{rated}} + C_2 \cdot F_{PTO_{rated}} \tag{21}$$

Here, C_0 represents engineering costs, C_1 is related with the rated force and the number of scalable modular PTO units, C_2 is related with the length of the translator, $S_{PTO_{rated}}$ represents the PTO rated stroke, and $F_{PTO_{rated}}$ the rated force.

Fig. 5a shows a scheme of the AMSRM module and its main parts: translator and stator. This type of electric machine can be designed based on stacking a certain number of modules (or stators), where the total force is the result of multiplying the number of modules by the nominal force of one module. The stroke of the electric machine is related to the number of stator modules and the total length of the translator, including the nominal stroke. For this reason, in a particular PTO solution, stroke and force can be selected independently, and similarly, in the cost function, stroke and force appear to be independent terms.

Fig. 5b shows a plot with the relationship between PTO costs and PTO force for different PTO designs. In this case, the cost evaluation is simplified, based on manufacturing data of SEATITAN project used in (Blanco et al., 2019), and normalized using the maximum budget as a base cost value. The direct relation between PTO force and PTO cost highlights the need for design strategies, such as optimizing the PTO design using a modular system, minimizing the dimensions of mechanical systems or using materials that reduce the weight.

This paper proposes a modular PTO design (see Section 4). The result of this approach is a versatile PTO which can be adapted to any type of WEC.

Fig. 6 presents the cost function used, based on quotations obtained from the development of the AMSRM prototype for various design of rated force and stroke, expressed in p.u. for confidentiality reasons (with 1 being the highest quotation obtained).

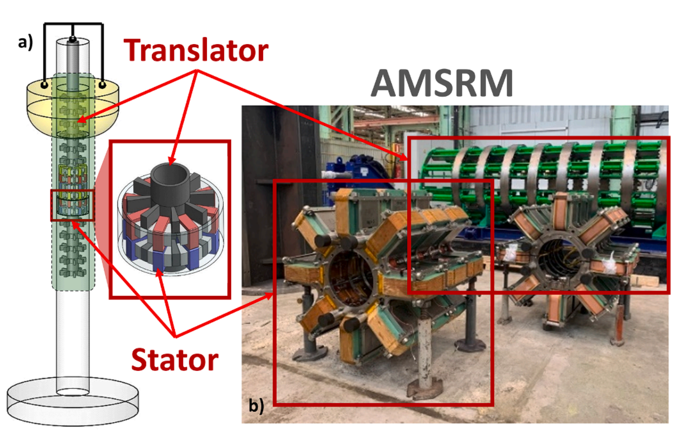

Fig. 5. (a) AMSRM module scheme developed in SEATITAN project integrated in a WEC; (b) Photograph of the.

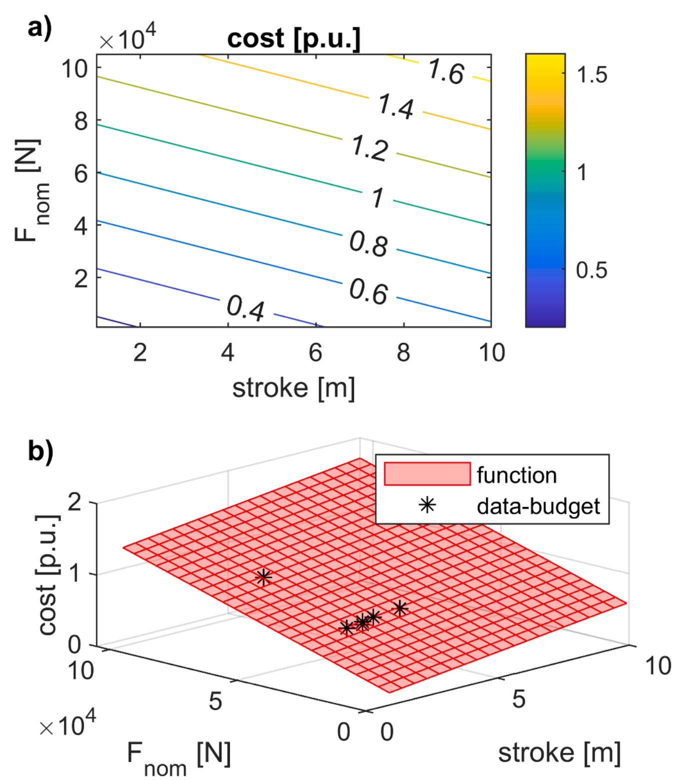

Fig. 6. Plot about the PTO costs function vs. PTO force and PTO stroke.

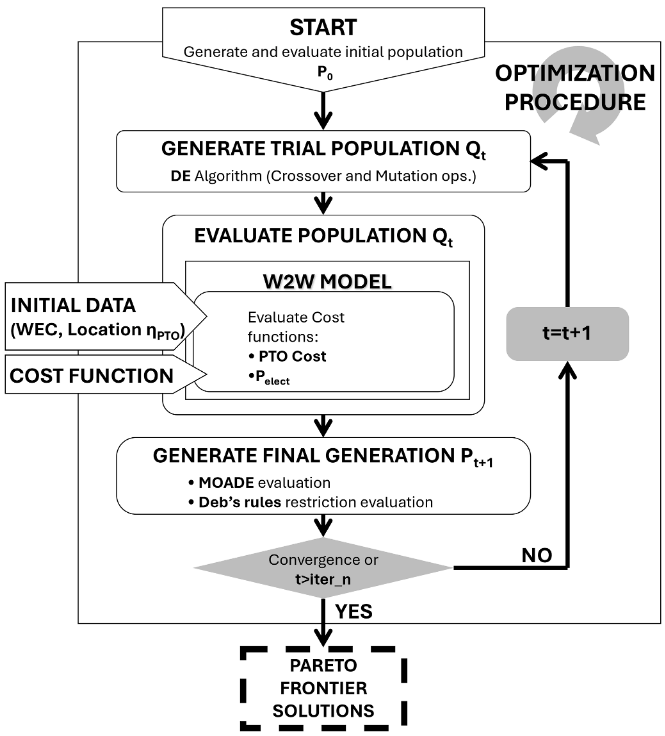

Fig. 7. Scheme of the optimization algorithm application.

Fig. 6a displays a contour plot representing the cost function value in per unit with respect to its input variables ($S_{PTO_{rated}}$ and $F_{PTO_{rated}}$). Fig. 6b shows the same information in a 3D plot, including the prototype quotations of the AMSRM marked with "*".

2.4.3. Optimization algorithm

The MODE algorithm operates as described in Fig. 7. The Target location and WEC type are predefined as supra-parameters (parameters that remains fixed during the optimization). Thus, one optimization or one execution of the POM has been carried out in each scenario, defined by WEC and target location. The "individuals" (solutions) are defined as PTO configuration, with specific values of each of the search space variables, force and stroke. For instance, individual no 1 could represent a PTO with 50 kN of force and 6 m of stroke). In the first "generation" (iteration), a random "population" (set) of individuals is defined, called $\mathbf{P_0}$. The W2W model, parametrised for a given WEC and using the information of every individual, is evaluated for every sea state of the chosen location. The results of the two objective functions for $\mathbf{P_0}$,

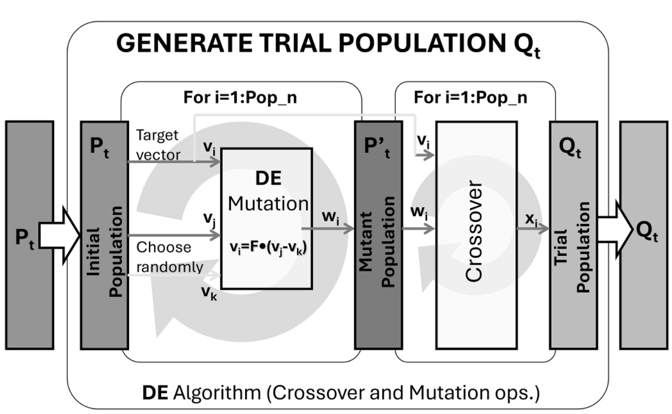

Fig. 8. Scheme of the Differential Evolutionary Algorithm to generate trial population Qt.

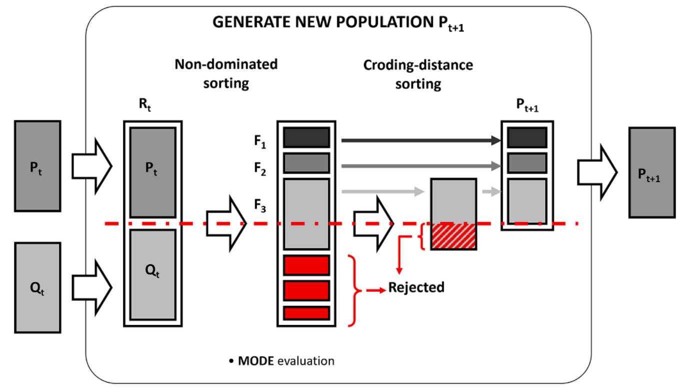

Fig. 9. Pareto Selection of the best options of [Qt,Pt] and to generate Pt+1.

obtained for each sea state, are: electrical power generated (weighted with the relative occurrence of each sea state) and PTO cost.

At this point, - considering an iteration or generation $t = 1$ - once the objective functions of each individual of a population P_t have been evaluated, the optimisation algorithm proceeds with the generation of a trial population Q_t. The values of the search space variables of each individual of the trial population Q_t are generated using the DE strategy (Mutation and crossover methods (Sirigu et al., 2020; Price and Storn, 2025)) based on the values of the initial population P_t (see Fig. 8). Every individual in the trial population Q_t is evaluated.

The best solution in the population sets Q_t and P_t are selected by means of the method that uses the algorithm NGSA-II (Srinivas and Deb, 1994; Zhou et al., 2011), based on the non-dominated sorting and the Crowding distance methods (see Fig. 9).

Since the optimisation problem is multi-objective, there is not a unique optimal solution, but a set of optimal solutions known as "Pareto front". Solutions on the Pareto front are optimal because there is no other better solution in both objective functions. All these solutions satisfy the conditions of maximizing the electrical power production and minimizing the PTO cost.

3. PTO design results obtained VIA POM

This section summarizes the results of the PTO design obtained using POM. Eight case study scenarios (combination of WEC type and location) have been considered, taking into account two different locations for each of the four WEC types evaluated (see Table 1): a semi-submerged single body point absorber (i.e. inspired by its working principle) similar to CORPOWER technology (CORPOWER Homepage 2025) (CPwec - Fig. 2a); a single body point absorber with structure fixed to the sea bed, similar to SEACAP technology (HYDROCAP ENERGY homepage 2025) (SCwec - Fig. 2a); a multibody set of point absorbers with a common structure, similar to CENTIPOD technology (CENTIPOD homepage 2025) (CNwec - Fig. 2c); and a two-body point absorber with a buoy and a plate, similar to WEDGE technology (WEDGE Global Homepage 2025) (WGwec - Fig. 2b). The locations considered correspond to the test facilities: Aguaçadoura (Portugal

Table 1
Scenarios to be analysed with the POM.

N°. scenario	WEC technology	Location
1	CP – CorPower (CorPower WEC)	1 – Aguaçadoura
2	CP – CorPower (CorPower WEC)	2 – BiliaCroo
3	SC – SeaCap (HydroCap WEC)	1 – Orkney
4	SC – SeaCap (HydroCap WEC)	2 – Semrev
5	CN – Centipod (Centipod WEC)	1 – BiliaCroo
6	CN – Centipod (Centipod WEC)	2 – BiMEP
7	WG – W1 (WedgeGlobal WEC)	1 – Plocan
8	WG – W1 (WedgeGlobal WEC)	2– BiMEP

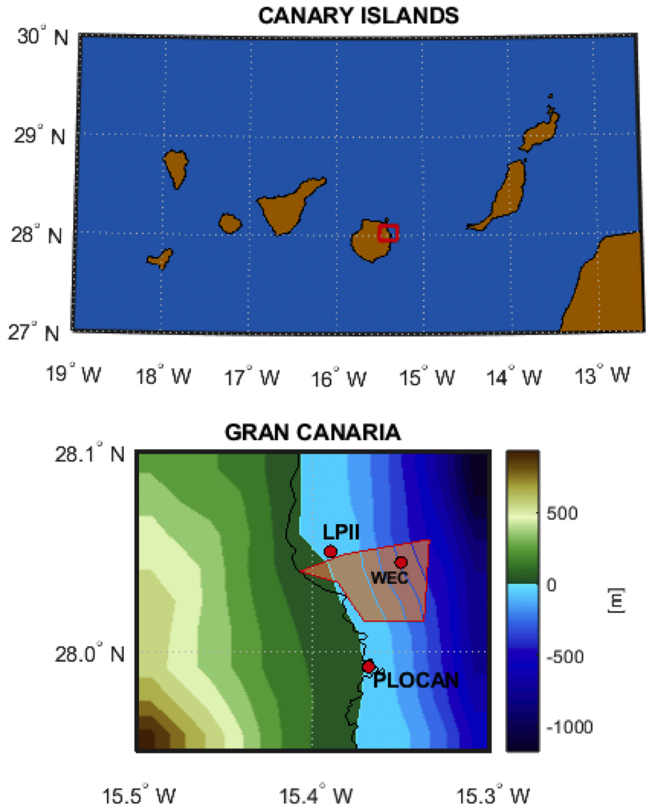

Fig. 10. PLOCAN location and scatter diagram.

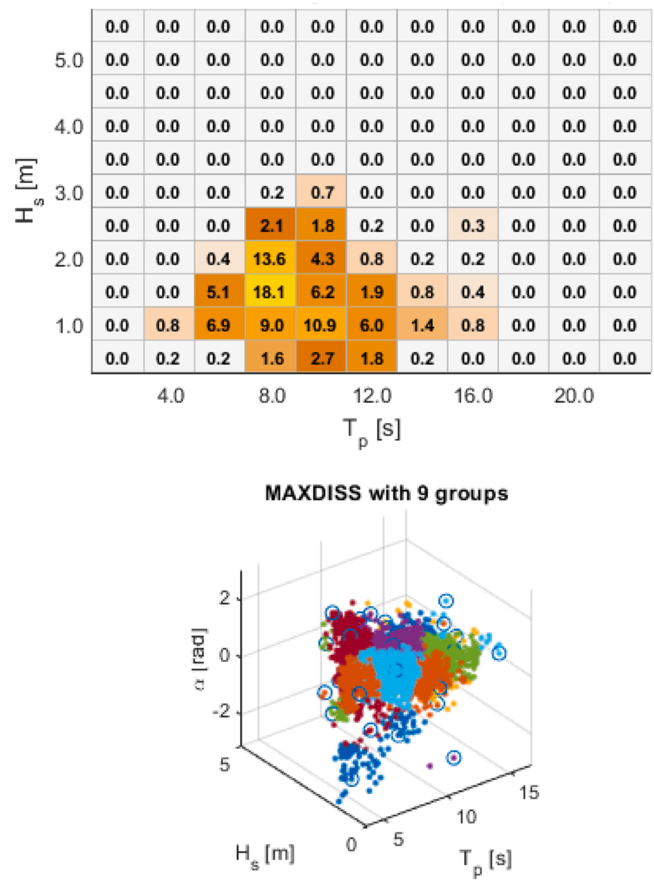

Fig. 11. Scatter diagram and the nine sea states selected by MAXDISS for the PTO characterization methodology.

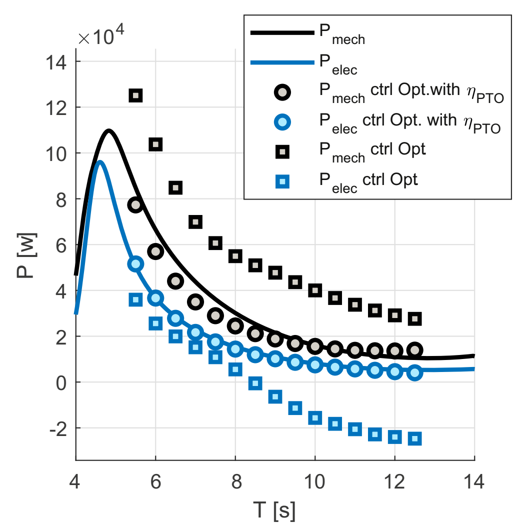

Fig. 12. Electrical and mechanical power profiles for different input wave periods, and with two energy extraction controls.

(WEDGE Global Homepage 2025), Bilia Croo Bilia Croo (UK – EMEC (WEDGE Global Homepage 2025), Orkney (UK – EMEC (WEDGE Global S.L. Homepage 2025), Semrev (France – Nantes (M. WEDGE Global S.L. Homepage 2025), BIMEP (Spain – Vasque Country (WEDGE Global S.L. Homepage 2025) and PLOCAN (Spain – Canary Islands) (WEDGE Global Homepage 2025). These eight scenarios are summarised in Table 1.

For a better understanding of the POM, the results for the specific scenario 7 (Table 1) are presented first. This scenario corresponds to the two-body point absorber WGwec (WEDGE Global Homepage 2025) at PLOCAN (WEDGE Global Homepage 2025) location, a test site in the Canary Islands (Spain). Using this case as an example, a selection methodology for the optimum solution is explained (see Section 3.1). The optimal solution is defined as the ideal values for the PTO parameters: stroke and power. This solution satisfies the optimization objective functions: max P_{elec} (13) and min *cost* (21).

3.1. Exemplification of POM execution: results for one base case

In a first stage, the methodology is applied simulating 9 representative sea states of the target location of the WEC device to evaluate the power extraction profile. In scenario 7, the location is PLOCAN (Fig. 10 and Fig. 11 show the sea location and the corresponding scatter diagram respectively). The sea states of the location are selected using a MAXDISS algorithm, as described in (De Andrés et al., 2013). This approach reduces the number of sea states evaluated and simplifies the graphical representation of the results. A wave elevation time profile is generated considering the H_s (significant height) and T_p (peak period) of the sea state and a JONSWAP spectrum (Hasselman, 1973)

3.1.1. Preliminary analysis of optimum control: maximization of mechanical power vs. maximization of electrical power in regular waves

As a preliminary analysis of the WEC operating under the optimum control proposed in Section 2.1, the W2W tool is used with regular waves in order to obtain the WEC power output profiles (mechanical and electrical) for different input wave periods, as shown in Fig. 12. The power profiles for two cases are presented: (blue lines stand for mechanical power and brown lines stand for electrical power): (1) the lines marked with squares represents the case where the control does not account for the PTO losses; (2) the lines marked with circles correspond to the case where the PTO energy extraction control has been modified to take into account PTO losses. The PTO efficiency considered is 75 %.

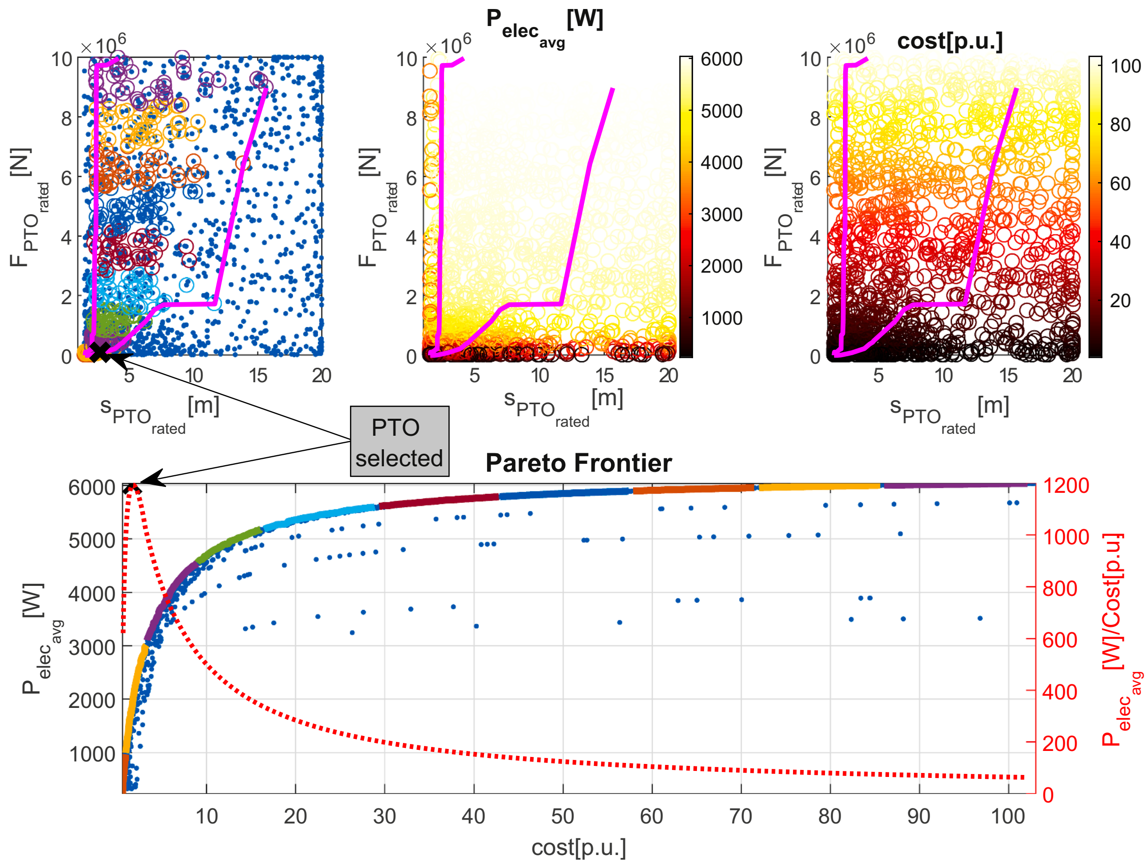

Fig. 13. Pareto front of scenario 7: a) b) c) PTO solutions respect to the search space variables (rated force and stroke of the PTO); d) PTO solutions respect to the optimization functions (annual average power of the PTO and PTO cost).

This figure shows that in case (1), more mechanical power is extracted, but the excessive reactive mechanical power reduces the electric power generated. In some frequencies, the electric power even reaches negative values, which means that the system requires electric power from the grid to compensate the power losses.

3.1.2. POM exemplification: execution of POM in scenario 7 (Table 1; 2-body point absorber at plocan facility location) in irregular waves

In a second stage, the multi-objective optimization algorithm phase of the POM is executed under irregular waves, considering the $F_{PTO_{rated}}$ and S_{PTO} as the search space variables, with the objective functions max (P_{ele}) and min ($cost_{PTO}$). However, due to preliminary information such as the PTO cost and efficiency, the ratio of generated power to cost is used in this case, which is inversely proportional to a PTO CAPEX/kW figure. The best selection criterion is the ratio of "generated electrical power" to "PTO cost". Nevertheless, this criterion can be adjusted according to the technology developers' needs by adding technical constraints, such as setting a maximum rated stroke or choosing the best solution from the Pareto front in terms of the Levelized Cost of Electricity (LCOE).

The graphical results of the execution of the POM for scenario 7 are shown in Fig. 13. Fig. 13a–c represent the PTO solutions respect to the search space variables (rated force - $F_{PTO_{rated}}$(N) - and stroke of the PTO - $S_{PTO_{rated}}$ (m) -); d) PTO solutions respect to the optimization functions (annual average power of the PTO - $P_{elecavg}$(W) - and PTO cost - costs (p.u) -).

In Fig. 13a, the represented PTO solutions are blue points if it not belongs to Pareto front, or circles if it belongs to the Pareto front (the colour of the circle correspond with the colour of the section of the Pareto front represented in Fig. 13d). In Fig. 13b, each PTO solutions are represented with a circle which colour is the value of the objective function annual average power of the PTO. In Fig. 13c, each PTO solutions are represented with a circle which colour is the value of the objective function PTO cost. The magenta curve plotted in these three graphs (Fig. 13a–c) in the search space represent the zone of PTO solutions that belongs to the Pareto front. Fig. 13d represents the set of realizable solutions in the space of the objective functions ($P_{elecavg}$(W) and costs (p.u)) by representing the Pareto front.

Finally, in Fig. 13d, the PTO solutions (respect to the objective functions) are plotted as blue points and a well-defined Pareto front can be observed (divided into different sections remarked with different colours). The optimal PTO solution point is highlighted in both the search space (Fig. 13a) and the objective function space (Fig. 13d) with a black "X" marker. In Fig. 13d, the relationship between $P_{elecavg}$ (W) and costs (p.u) is also represented by the red dashed line, where the selected PTO solution (selected in form the Pareto Fortier solutions) is the PTO configuration with best $P_{elecavg}/cost$ ratio. The optimal solution is found at 109.26 kN of rated force and 2.664 m of maximum stroke.

Table 2
PTO configurations selected in each scenario.

N°. scenario	WEC	Location	$F_{PTO_{rated}}$ [kN]	S_{PTO} [m]
1	CP	1	298.41	4.335
2	CP	2	260.97	3.205
3	SC	1	383.24	2.437
4	SC	2	236.36	2.332
5	CN	1	291.92	1.874
6	CN	2	269.10	2.961
7	WG	1	109.26	2.664
8	WG	2	144.66	2.273

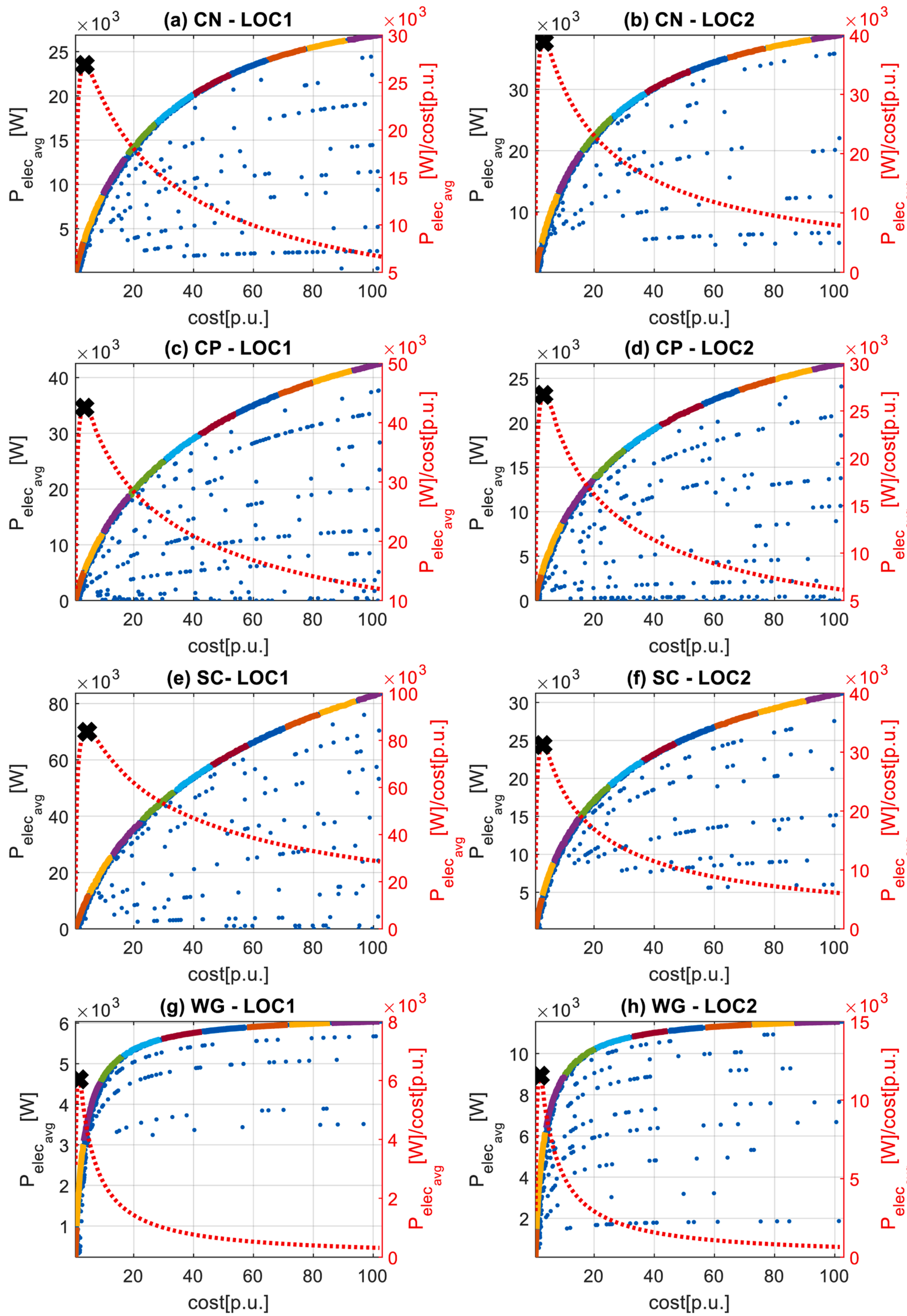

Fig. 14. Pareto front of the eight scenarios.

3.2. Results of the POM execution for all considered cases

The criterion for selecting the optimal solution after the execution of the POM has been chosen considering the differences in the ratio between the average power ($P_{average}$[W]) and PTO cost (cost [p.u.]) that different WEC technologies may exhibit. This ratio may change depending on the PTO characteristics of each technology, such as weight or dimensions. The Pareto fronts have been obtained for the eight scenarios studied (see Fig. 1-Annex). For all eight scenarios analysed, the optimal solutions continue to belong to the Pareto front obtained after the execution of the POM. As shown in Fig. 1 (Annex), although the configuration of the PTO can change in each case, it will still belong to the Pareto front of solutions identified after executing the POM. Table 2 summarizes the force and stroke values for the selected PTOs for each scenario, which corresponds to the PTO solution with the highest power-to-cost ratio.

The Fig. 14 shows the PTO solutions evaluated in each of the eight scenarios, representing in each scenario: the set of realizable solutions in the space of the objective functions ($P_{elecavg}$(W) and costs (p.u)) in blue points, and the Pareto front (divided into different sections remarked with different colours); the line $P_{elecavg}/cost$ ratio is represented by the red dashed line; and the optima PTO solution (selected as the best $P_{elecavg}/cost$ ratio solution) is with a black "X" marker. The Table 2 results are based in the plots of this Fig. 14.

4. Application of POM results: selection of the AMSRM module to build the full PTO

Section 2.3 presented the relationship between the number of

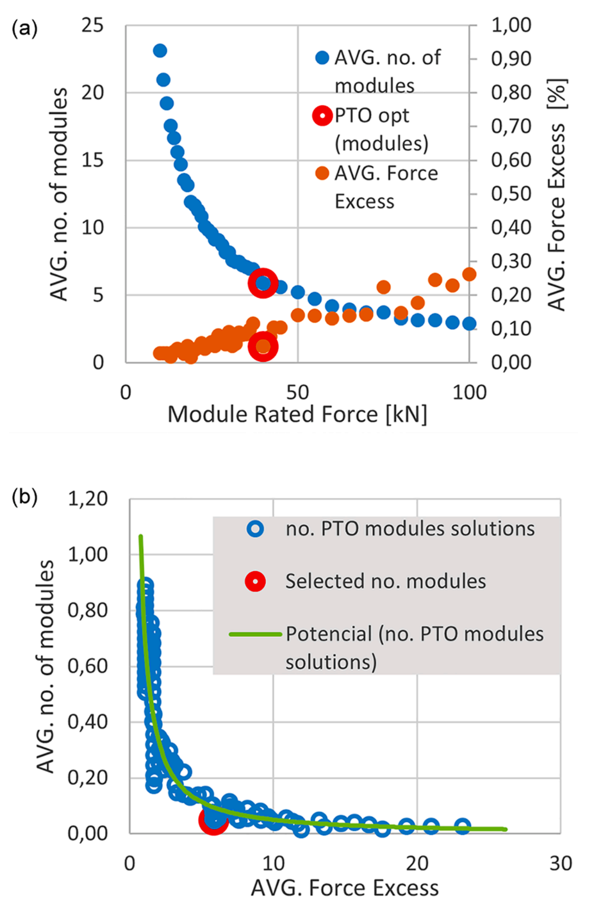

Fig. 15. (a) Average number (of 8 scenarios) of PTO modules, and Force excess for different configurations of PTO (different values of rated force of PTO module). (b) Average number of PTO modules vs. Force excess.

generator modules and the final P_{elec} (W) of the PTO, as well as its influence on the PTO *costs* (see Fig. 5). Section 3 demonstrated the influence of the decision variables ($F_{PTO_{rated}}$ (kN) and S_{PTO} (m)) in obtaining the optimal PTO solution that satisfies the POM objective functions to achieve max P_{elec} and min *costs*. Consequently, the optimal number of generator modules was obtained using the POM Blanco and Lafoz (2025).

Section 4 presents a case study applying the results obtained from executing of the POM for the eight case-study scenarios. The results in Table 2 were used to design an optimal PTO solution that addresses all eight scenarios. This design was evaluated based on the characteristics of the AMSRM modules.

For this study, a range of AMSRM modules was evaluated, offering rated forces between 10 and 400 kN. The variables considered in designing the complete PTO are:

- Number of modules: This was minimised to simplify the PTO. Moreover, since the total generator length depends on the stroke and the number of modules, reducing the number of modules helps to fit the PTO within the available space in the WEC.
- Excess in resulting force: The over-dimensioning of the PTO caused by the integer nature of the number of modules count was also minimised.

Fig. 15a presents the results for various PTO configurations across the 8 scenarios. The average number of modules (blue line) and the nominal force for each module (kN) are shown, along with the average force excess percentage (%) relative to the optimal force calculated by the POM (orange line). Using the double-criteria approach - minimizing both the number of modules and force oversizing -, Fig. 15 highlights a compromise solution consisting of a 40- kN module. This configuration balances PTO force excess across the 8 scenarios while maintaining a relatively low average number of modules (see red point). Fig. 15b presents the average number of modules vs. the average force excess percentage (%) showing the selected rated force of the module as a red point). The complete numerical results are included in Table 3.

A nominal efficiency of 85 % was assumed in all the cases presented in the figure. This value was derived from the preliminary electromagnetic model of the linear generator considered (AMSRM) (Blanco et al., 2021)

In a final step, the influence of PTO efficiency on the results was evaluated. Based on the methodology, the rated force value of the AMSRM module was determined to be 40 kN. However, the actual efficiency may differ from the design phase value when applied to a real AMSRM prototype. This variation could result from factors such as modifications to the magnetic circuit due to mechanical implementation requirements or an increase in conduction resistance caused by electrical connections.

The module selection analysis was repeated for alternative efficiency values to assess the impact the impact of this variable on the results. Table 3 presents the results of the parametric analysis OFAT (one factor at time sensitivity analysis) of the AMSRM module force. The base efficiency value was set at 85 %.

The variables FPTO and the number of AMSRM modules were chosen to analyze how different efficiency values affect the system. These variables, determined by the POM, define and limit the characteristics of the AMSRM generator. Their changes were evaluated relative to the selected base efficiency.

The results show that as efficiency decreases, the required nominal PTO force increases. However, this only leads to a small increase of 1–2 AMSRM modules to meet the required force in each scenario. For CP technology at location 2 (BiliaCroo), no additional modules are needed

As future works, it would be possible to analyse the sensitivity of the POM results according to different aspects that may vary from the early design stage where the POM would be used to the manufacturing stages. As the same way of the impact of the efficiency of the PTO loss model has

Table 3
Percentage of PTO characteristics variation and of the objective functions with respect to a variation in the AMSRM efficiency (OFAT [one factor at a time] sensitivity analysis).

SCENARIO		OFAT nu (F_pto analysis)							
WEC	no. _location	F_{pto} (η: 75 %)	F_{pto} (η: 80 %)	F_{pto} (η: 85 %)	no. pto modules (η: 75 %)	no. pto modules (η: 80 %)	no. pto modules (η: 85 %)	Δno (nu:75 %)	Δno (nu:80 %)
CN	1	361,0	325,0	**291,9**	10	9	**8**	2	1
CP	1	327,9	300,5	**298,4**	9	8	**8**	1	0
SC	1	418,2	413,6	**383,2**	11	11	**10**	1	1
WG	1	140,0	128,9	**109,3**	4	4	**3**	1	1
CN	2	306,7	290,5	**269,1**	8	8	**7**	1	1
CP	2	264,5	278,0	**261,0**	7	7	**7**	0	0
SC	2	291,1	274,0	236,4	8	7	6	2	1
WG	2	163,8	148,3	144,7	5	4	4	1	0

already been analysed, other variations such as variations in the parameters of the PTO cost model can be analysed. In this case, for example, it can be expected that, as with variable efficiency, variations in the PTO cost model will affect all solutions equally, causing the optimal values to remain stable or vary only slightly.

5. Conclusions

From the perspective of computational tools, the analysis presented in this paper concludes that the POM is a valuable design tool for optimizing WEC design. The proposed POM establishes a universal methodology that can be adapted and applied to any type of WEC technology and location. This statement is supported by the results obtained from its application to 8 different scenarios, involving 4 distinct technologies and 2 sea locations. Consistent and positive results were obtained, as evidenced in the Pareto front solution graphs and the optimal PTO selection graphs.

Additionally, this study confirms that the POM is a highly applicable design tool. By applying the POM results to the modular design of the particular linear generator topology AMSRM as part of the PTO design optimization, a balanced solution is achieved for all 8 scenarios. This solution exhibits common design characteristics, such as a PTO force per module (F_{PTO} per module) of 40 kN and a specific number of modules. These results highlight the versatility of the design which maximizes electrical output power, P_{elec} (max) while minimizing the PTO costs (CAPEX). Specifically, the application of the POM reveals information about a design parameter that influences the length of the PTO, the stroke (S_{PTO}). The analysis of S_{PTO} underscores the importance of this parameter, as it influences not only the minimization of CAPEX but also the determination of the optimal modular system design.

Finally, the sensitivity analysis of PTO efficiency indicates that the selection of the maximum force and stroke remains relatively stable despite potential variations in the efficiency.

In conclusion, this study demonstrates that optimization algorithms, when integrated into an appropriate methodology and computational environment, are powerful mathematical tools that contribute significantly to WEC design. This has been clearly illustrated through the POM proposed in this study.

The POM methodology described in this study presents several considerations or limitations that must be taken into account when analysing the results obtained. It was implemented using a simplified cost, loss, and dynamic model of the PTO. However, these simplifications could be considered acceptable due to the initial design phase where the POM will be used. Considering these limitations and the work developed, future work is focused on improving the POM by incorporating different types of PTOs (which would allow a more accurate representation of different power conversion systems), including economic models (LCOE estimation and techno-economic parameters), or integrating the POM into WEC or wave farm design tools (analysing the same PTO for different WEC concepts). In addition, the POM could be used to perform sensitivity analysis of the linear generator over a wide range of locations, or perform sensitivity analysis of the POM results as a function of different aspects that may vary from the initial design phase - where the POM would be used - to the manufacturing phases (such as the efficiency value or that of the cost model parameters).

Funding

This research, developed under the Projects SETITAN (ID: 764014) and MARES (ID: 101172746), has received funding from European Union's Horizon 2020 research and innovation programme under H2020-EU.3.3.2. - Low-cost, lowcarbon energy supply (LCE-07–2016–2017) and from European Union's Horizon Europe research and innovation programme under HORIZON-CL5-2024-D3-01-10 - Next generation of renewable energy technologies, respectively.

CRediT authorship contribution statement

Marcos Blanco: Writing – review & editing, Writing – original draft, Visualization, Software, Project administration, Methodology, Investigation, Funding acquisition, Formal analysis, Conceptualization. **Isabel Villalba:** Writing – review & editing, Writing – original draft, Visualization, Software, Methodology, Investigation, Conceptualization. **Marcos Lafoz:** Writing – review & editing, Writing – original draft, Supervision, Resources, Project administration, Investigation, Funding acquisition. **Jorge Nájera:** Writing – review & editing, Validation, Software, Formal analysis. **Gustavo Navarro:** Resources, Methodology, Investigation. **Miguel Santos-Herrán:** Validation, Methodology, Formal analysis, Conceptualization.

Declaration of competing interest

The authors declare that they have no known competing financial interests or personal relationships that could have appeared to influence the work reported in this paper.

Acknowledgments

The authors would like to thank WavEC Renewables Offshore and, in particular, the researcher Mr. Miguel Vicente, for all the support provided in the hydrodynamic modelling of the wave energy converters integrated into the final code, as well as the WEC developers participating as partners in SEATITAN.

References

Ahamed, R., McKee, K., Howard, I., 2020. Advancements of wave energy converters based on power take off (PTO) systems: a review. Ocean Eng. 204, 107248. https://doi.org/10.1016/j.oceaneng.2020.107248 (May).

Ahamed, R., McKee, K., Howard, I., 2022. A Review of the Linear Generator Type of Wave Energy Converters' Power Take-Off Systems. MDPI. https://doi.org/10.3390/su14169936. Aug. 01.

Alves, M., 2012. Numerical Simulation of the Dynamics of Point Absorber Wave Energy Converters Using Frequency and Time Domain Approaches. Instituto Superior Técnico- Universidad Técnica de Lisboa, Lisboa.

Amini, E., et al., 2022. Optimization of hydraulic power take-off system settings for point absorber wave energy converter. Renew. Energy 194, 938–954. https://doi.org/10.1016/j.renene.2022.05.164.

Balaji V.S.S., Saravanan R., and Chandrasekaran G., "Multiobjective design optimization of power take-off (PTO) gear box through NSGA II," Dec. 08, 2020, CRC Press. 10.1201/9781003081166-5.

Bechlenberg, A., Wei, Y., Jayawardhana, B., Vakis, A.I., 2023. Analysing the influence of power take-off adaptability on the power extraction of dense wave energy converter arrays. Renew. Energy 211, 1–12. https://doi.org/10.1016/j.renene.2023.04.076.

Blanco, M., et al., 2019b. Implementation of an energy extraction control including PTO-losses in a complete WEC model for PTO design procedure. In: Proceedings of the 13th European Wave Tidal Energy Conference (EWTEC). Napoles.

Blanco, M., et al., 2021b. Simplified model of a novel direct-drive PTO based on an azimuthal linear switched reluctance generator. In: Proceedings of the 14th European Wave and Tidal Energy Conference (EWTEC). Plymouth (UK).

Blanco, M., et al., 2021a. Meta-heuristic optimisation approach for wave energy converter design by means of a stochastic hydrodynamic model. IET Renew. Power Gener. 15 (3), 548–561. https://doi.org/10.1049/rpg2.12021.

Blanco, M., Lafoz, M., Álvarez, A., Herreros, I., 2011. Multi-objective differential evolutionary algorithm for preliminary design of a direct-drive power take-off. In: Proceedings of the Ninth European Wave and Tidal Energy Conference (EWTEC). Southampton (UK).

Blanco M., Lafoz M., and García Tabares L., "Laboratory tests of linear electric machines for wave energy applications with emulation of wave energy converters and sea waves. 2025.".

Blanco, M., Lafoz, M., Ramirez, D., Navarro, G., Torres, J., Garcia-Tabares, L., 2019a. Dimensioning of point absorbers for wave energy conversion by means of differential evolutionary algorithms. IEEe Trans. Sustain. Energy 10 (3), 1076–1085. https://doi.org/10.1109/TSTE.2018.2860462.

Blanco, M., Moreno-Torres, P., Lafoz, M., Ramírez, D., 2015. Design parameter analysis of point absorber WEC via an evolutionary-algorithm-based dimensioning tool. Energies 8 (10), 11203–11233. https://doi.org/10.3390/en81011203. . (Basel).

Cagney D., "2030 ocean energy vision. Industry analysis of future deployments, costs and supply chains," 2022.

Carstensen, C., 2008. Eddy Currents in Windings of Switched Reluctance Machines. Aachen University, Aachen (Germany).

"CENTIPOD homepage", Accessed: Mar. 22, 2025. [Online]. Available: http://www.ecomerittech.com/centipod.php.

Chang, G., Jones, C.A., Roberts, J.D., Neary, V.S., 2018. A comprehensive evaluation of factors affecting the levelized cost of wave energy conversion projects. Renew. Energy 127, 344–354. https://doi.org/10.1016/j.renene.2018.04.071.

Conill Y., "Ocean energy key trends and statistics ," 2022.

"CORPOWER Homepage." Accessed: Mar. 22, 2025. [Online]. Available: http://www.corpowerocean.com/.

Cummins W., "The impulse response function and ship motions," 1962.

Davidson, J., Genest, R., Ringwood, J.V., 2018. Adaptive control of a wave energy converter. IEEe Trans. Sustain. Energy 9 (4), 1588–1595. https://doi.org/10.1109/TSTE.2018.2798921.

de A.F. Falcão O., "Wave energy utilization: a review of the technologies," Apr. 2010. 10.1016/j.rser.2009.11.003.

de Andrés, A.D., Guanche, R., Armesto, J.A., del Jesus, F., Vidal, C., Losada, I.J., 2013. Time domain model for a two-body heave converter: model and applications. Ocean Eng. 72, 116–123. https://doi.org/10.1016/j.oceaneng.2013.06.019.

De Andrés, A.D., Guanche, R., Armesto, J.A., Del Jesus, F., Vidal, C., Losada, I.J., 2013. Time domain model for a two-body heave converter: model and applications. Ocean Eng. 72, 116–123. https://doi.org/10.1016/j.oceaneng.2013.06.019.

El Montoya Andrade, D., De La Villa Jaén, A., García Santana, A., 2014. Considering linear generator copper losses on model predictive control for a point absorber wave energy converter. Energy Convers. Manag. 78, 173–183. https://doi.org/10.1016/j.enconman.2013.10.037.

Faiz, J., Nematsaberi, A., 2017. Linear electrical generator topologies for direct-drive marine wave energy conversionan overview. IET Renewable Power Generation. Institution of Engineering and Technology, pp. 1163–1176. https://doi.org/10.1049/iet-rpg.2016.0726.

Falnes, J., 1999. Wave-energy conversion through relative motion between two single-mode oscillating bodies. J. Offshore Mech. Arct. Eng. 121 (1), 32–38. https://doi.org/10.1115/1.2829552.

Falnes, J., 2002. Ocean Waves and Oscillating Systems, Linear Interactions Including Wave-Energy Extraction. Cambridge University Press. https://doi.org/10.1017/CBO9780511754630.

García, F., Lafoz, M., Blanco, M., García-Tabares, L., 2011. Efficiency calculation of a direct-drive power take-off. In: Proceedings of the 9th European Wave and Tidal Energy Conference (EWTEC). Southampton (UK).

Genest, R., Bonnefoy, F., Clément, A.H., Babarit, A., 2014. Effect of non-ideal power take-off on the energy absorption of a reactively controlled one degree of freedom wave energy converter. Appl. Ocean Res. 48, 236–243. https://doi.org/10.1016/j.apor.2014.09.001.

Grainger, J., Stevenson, W., 1994. Power System Analysis. McGraw-Hill, New York, NY, USA; London, UK.

Gunn, K., Stock-Williams, C., 2012. Quantifying the global wave power resource. Renew. Energy 44, 296–304. https://doi.org/10.1016/j.renene.2012.01.101.

Guo, C., Sheng, W., De Silva, D.G., Aggidis, G., 2023. A Review of the Levelized Cost of Wave Energy Based on a Techno-Economic Model. MDPI. https://doi.org/10.3390/en16052144. Mar. 01.

Hals, J., Falnes, J., Moan, T., 2011. A comparison of selected strategies for adaptive control of wave energy converters. J. Offshore Mech. Arct. Eng. 133, 31101. https://doi.org/10.1115/1.4002735.

Hasselman K., "Measurements of wind-wave growth and swell decay during the joint North Sea wave project (JONSWAP)," 1973.

He, Z., Ning, D., Gou, Y., Mayon, R., 2022b. Optimization of a wave energy converter square array based on the differential evolution algorithm. Ocean Eng. 262. https://doi.org/10.1016/j.oceaneng.2022.112189.

He, Z., Ning, D., Gou, Y., Zhou, Z., 2022a. Wave energy converter optimization based on differential evolution algorithm. Energy 246. https://doi.org/10.1016/j.energy.2022.123433.

"HYDROCAP ENERGY homepage." Accessed: Mar. 22, 2025. [Online]. Available: https://hydrocap.com/.

I. I. R. E. A. O. E. Europe, "Scaling up investments in ocean energy technologies," 2023.

"Surging wave energy absorption through increasing thrust and efficiency (SEA TITAN)." Accessed: Mar. 22, 2025. [Online]. Available: https://seatitan.eu/.

Lee C., "WAMIT theory manual," 1995.

Maria-Arenas, A., Garrido, A.J., Rusu, E., Garrido, I., 2019. Control strategies applied to wave energy converters: state of the art. Energies 12 (16). https://doi.org/10.3390/en12163115. . (Basel).

Mørk, G., Barstow, S., Kabuth, A., Pontes, M.T., 2010. Assessing the global wave energy potential. In: Proceedings of the International Conference on Offshore Mechanics and Arctic Engineering - OMAE, pp. 447–454. https://doi.org/10.1115/OMAE2010-20473.

Pecher, A., Kofoed, J.P., 2017. Handbook of Ocean Wave Energy, 7. Springer International Publishing.

Penalba, M., Ringwood, J., 2016b. A review of wave-to-wire models for wave energy converters. Energies 9 (7), 506. https://doi.org/10.3390/en9070506. . (Basel).

Penalba, M., Ringwood, J.V., 2016a. A Review of Wave-To-Wire Models For Wave Energy Converters. MDPI AG. https://doi.org/10.3390/en9070506. Jul. 01.

Price K. and Storn R., "Differential evolution," Dr. Dobb's Journal. Accessed: Mar. 22, 2025. [Online]. Available: https://www.drdobbs.com/database/differential-evolution/184410166.

Sadiku, M.N., Alexander, C.K., 2007. Fundamentals of Electric Circuits. McGraw-Hill Higher Education.

Saveca, J., Sun, Y., Wang, Z., 2022. A hybrid multiobjective optimization based on nondominated sorting and crowding distance, with applications to wave energy converters. Int. Trans. Electr. Energy Syst. 2022, 1–18. https://doi.org/10.1155/2022/8309697.

Sirigu, S.A., et al., 2020. Techno-economic optimisation for a wave energy converter via genetic algorithm. J. Mar. Sci. Eng. 8 (8). https://doi.org/10.3390/JMSE8070482.

Srinivas, N., Deb, K., 1994. Muiltiobjective optimization using nondominated sorting in genetic algorithms. Evol. Comput. 2 (3), 221–248. https://doi.org/10.1162/evco.1994.2.3.221.

Tan, J., Polinder, H., Jarquin Laguna, A., Miedema, S., 2022. The application of the spectral domain modeling to the power take-off sizing of heaving wave energy converters. Appl. Ocean Res. 122, 103110. https://doi.org/10.1016/j.apor.2022.103110.

Tan, J., Polinder, H., Laguna, A.J., Wellens, P., Miedema, S.A., 2021a. The influence of sizing of wave energy converters on the techno-economic performance. J. Mar. Sci. Eng. 9 (1), 1–25. https://doi.org/10.3390/jmse9010052.

Tan, J., Wang, X., Laguna, A.J., Polinder, H., Miedema, S., 2021b. The influence of linear permanent magnet generator sizing on the techno-economic performance of a wave energy converter. In: Proceedings of the 2021 13th International Symposium on Linear Drives for Industry Applications, LDIA 2021. Institute of Electrical and Electronics Engineers Inc. https://doi.org/10.1109/LDIA49489.2021.9505880

Tedeschi, E., Molinas, M., 2012. Tunable control strategy for wave energy converters with limited power takeoff rating. IEEE Trans. Ind. Electron. 59 (10), 3838–3846. https://doi.org/10.1109/TIE.2011.2181131.

Torres, J., Moreno-Torres, P., Navarro, G., Blanco, M., Lafoz, M., 2018. Fast energy storage systems comparison in terms of energy efficiency for a specific application. IEEE Access 40656–40672. https://doi.org/10.1109/ACCESS.2018.2854915.

"WEDGE Global S.L. Homepage." Accessed: Mar. 22, 2025a. [Online]. Available: http://wedgeglobal.com/.</bib>.

"Plataforma Oceánica de Canarias (PLOCAN)." Accessed: Mar. 22, 2025f. [Online]. Available: https://plocan.eu/.

"Biscay marine energy platform (BIMEP)." Accessed: Mar. 22, 2025e. [Online]. Available: https://www.bimep.com/.

"Centrale Nantes offshore test site (SEMREV)." Accessed: Mar. 22, 2025d. [Online]. Available: https://sem-rev.ec-nantes.fr/.

"European Marine energy center (EMEC)." Accessed: Mar. 22, 2025c. [Online]. Available: https://www.emec.org.uk/facilities/wave-test-site/.

"Aguçadora test site." Accessed: Mar. 22, 2025b. [Online]. Available: https://www.wavec.org/en/test-sites/agucadora-test-sites.

Wehausen, J.V., 1967. Initial-value problem for the motion in an undulating sea of a body with fixed equilibrium position. J. Eng. Math. 1 (1), 1–17. https://doi.org/10.1007/BF01793635.

Yang, Bo, Duan, J., Chen, Y., Wu, S., Li, M., Cao, P., Jiang, L., 2024. A critical survey of power take-off systems based wave energy converters: summaries, advances, and perspectives. Ocean Eng. 298, 117149. https://doi.org/10.1016/j.oceaneng.2024.117149 (April).

Yu, Z., Falnes, J., 1995. State-space modelling of a vertical cylinder in heave. Appl. Ocean Res. 17 (5), 265–275. https://doi.org/10.1016/0141-1187(96)00002-8.

Yu, Z., Maceda, H., 1991. On the modelling of an OWC wave power system. J. Kansai Soc. Nav. Archit. (215), 123–128.

Zhang, J., Yu, H., Chen, M., 2023. Direct-drive wave energy conversion with linear generator: a review of research status and challenges. IET Renew. Power Gener. 17 (4), 1020–1034. https://doi.org/10.1049/rpg2.12637.

Zhou A., Qu B.Y., Li H., Zhao S.Z., Suganthan P.N., and Zhangd Q., "Multiobjective evolutionary algorithms: a survey of the state of the art," 2011, *Elsevier B.V.* 10.1016/j.swevo.2011.03.001.